THE JOURNAL OF PHYSICAL CHEMISTRY C

ARTICLE

pubs.acs.org/JPCC

A Method for Rapid Screening of Photosensitizers by Scanning Electrochemical Microscopy (SECM) and the Synthesis and Testing of a Porphyrin Sensitizer

Fen Zhang,[‡] Vladimir Roznyatovskiy,[†] Fu-Ren F. Fan,[†,‡] Vincent Lynch,[†] Jonathan L. Sessler,[*,†,§] and Allen J. Bard[*,†,‡]

[†]Department of Chemistry and Biochemistry, The University of Texas at Austin, Texas 78712, United States

[‡]Center for Electrochemistry and Department of Chemistry and Biochemistry, The University of Texas at Austin, Texas 78712, United States

[§]Department of Chemistry, Yonsei University, Seoul 120-749, South Korea

Supporting Information

ABSTRACT: A picoliter solution dispenser was used to fabricate photosensitizer arrays on mesoporous TiO_2 electrodes. The scanning electrochemical microscopy (SECM) technique, modified by replacing the usual ultramicroelectrode (UME) with an optical fiber and using the photooxidation of iodide in acetonitrile in a photoelectrochemical (PEC) cell, was shown to be useful for the initial screening of potential PEC photosensitizers. This SECM technique allows for the rapid identification of new dyes and also can be used to investigate the synergetic effect of multiple dyes for application in dye-sensitized solar cells (DSSCs). This technique was specifically demonstrated via the synthesis and analysis of a new, bis-bithiophene functionalized porphyrin derivative, wherein the modified SECM technique was used to carry out an initial test of its PEC efficiency relative to other dyes. The PEC properties of bulk films based on this new porphyrin derivative were then investigated and the results shown to be in good agreement with those obtained using the SECM method.

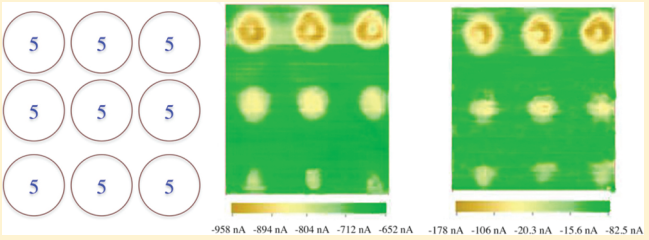

INTRODUCTION

Dye-sensitized solar cells (DSSCs) (also known as Grätzel cells) based on mesoporous TiO_2 electrodes have attracted extensive attention in recent years due to their expected low fabrication costs and relatively high efficiencies, η.[1,2] Although ruthenium polypyridyl complexes have proven to be excellent TiO_2 sensitizers and have achieved the high η values, up to 11.5%,[3] difficulties in large-scale manufacturing have been encountered. Ongoing efforts have been devoted to finding metal-free organic chromophores or inexpensive metal complexes that are suitable for use in DSSCs. In this context, porphyrins have been proven to be particularly attractive. These venerable chromophores bear analogy to pigments found in natural photosynthetic systems and are characterized by a Soret band in the 400−450 nm spectral region, as well as weaker Q bands centered around 550−600 nm but often extending over a greater spectral frequency.[4,5]

To date, scanning electrochemical microscopy (SECM) techniques have been applied in a number of areas,[6] including electrocatalyst and photocatalyst selection. For example, SECM-based approaches were used to screen bimetallic and trimetallic complexes as potential electrocatalysts for use in the oxygen reduction reaction (ORR). In fact, on the basis of SECM, we were able to identify several useful Pd−Co based electrocatalysts[7−10] that displayed activities in strong acid comparable to that of Pt. SECM methods have also been used to study oxygen evolution reactions.[11] Furthermore, by replacing the usual SECM ultramicroelectrode (UME) tip with an optical fiber, it proved possible to rapidly test potential semiconductor photocatalysts for use in photoelectrochemical (PEC) cells. In these latter screening studies, one end of the optical fiber was connected to a 150 W Xe lamp, and the other end was placed in the SECM tip holder over the spot array at a distance of about 100 μm. The photoactivity was determined from the photocurrent generated. This method was used to identify several good photocatalysts, including tungsten-doped bismuth vanadate, tin-doped iron oxide, and a number of others.[12,13]

In this paper, we demonstrate the feasibility of using the SECM method to screen arrays of DSSC photosensitizers prepared via a rapid deposition method on a TiO_2 nanotube substrate (anodized Ti). The arrays of photosensitizers in question are prepared from drop coating solutions using an automated dispenser on the TiO_2 nanotube substrate, as used in PEC experiments. For the present "proof of concept" study, we have synthesized a new functionalized

Received: November 2, 2010
Revised: December 13, 2010
Published: January 12, 2011

Scheme 1. Synthesis of Porphyrins 1 and 2a,b

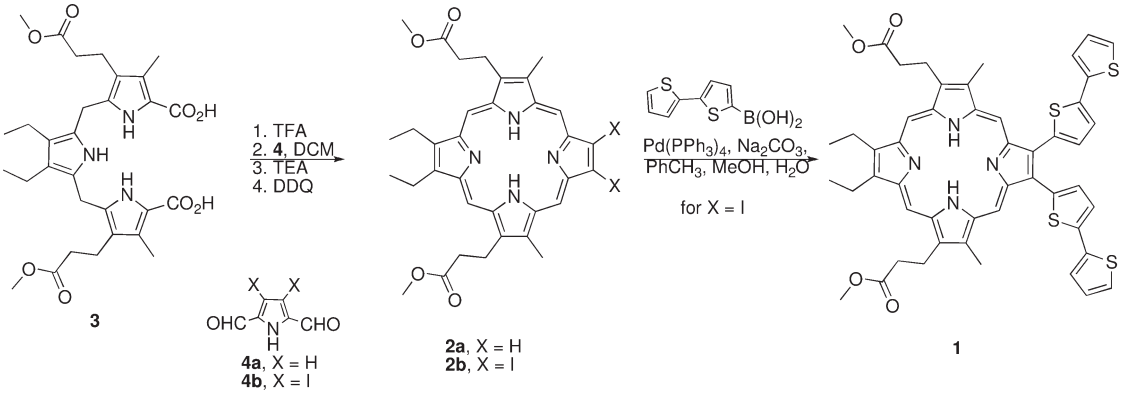

bis-bithiophene porphyrin derivative, **1**, and used it to prepare arrays of photosensitizer on an anodized TiO_2 nanotube substrate that were then tested using the modified SECM method. Photosensitizer arrays (consisting of spots on the TiO_2 nanotube substrate) were prepared from solutions of porphyrin **1**, as well from those of the control porphyrin system **2a** and the known PEC sensitizer, N719. The sensitized photocurrents of the constituent dyes (contained within the spots) were then measured by scanning an optical fiber over each spot on the array.

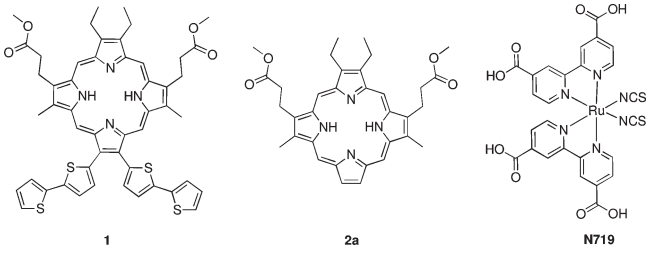

EXPERIMENTAL SECTION

Materials. Unless noted otherwise, chemicals used in this study were purchased commercially and used as received. 2,5-Diformylpyrrole, 3,4-diiodo-2,5-diformylpyrrole, and 2,2′-bithiophene-5-boronic acid were prepared according to published procedures.[14−16] *Cis*-bis(isothiocyanato)bis(2,2′-bipyridy-4,4′-dicarboxylato)-ruthenium(II)-bis-tetrabutyl ammonium (N719) was obtained from Aldrich. 21*H*,23*H*-Porphine-2,13-dipropanoic acid, 7,8-diethyl-3,12-dimethyl-17,18-di-(5-(2,2′-bithiophene)) dimethyl ester (**1**), 21*H*,23*H*-porphine-2,13-dipropanoic acid, 7,8-diethyl-3,12-dimethyl dimethyl ester (**2a**), and 21*H*,23*H*-porphine-2,13-dipropanoic acid, 7,8-diethyl-3,12-dimethyl-17,18-diiodo dimethyl ester (**2b**) were prepared as described below. Solutions of the dye N719 were prepared in ethanol at a concentration of 2×10^{-4} M. Solutions of porphyrins **1** and **2a**, also studied as dyes (vide infra), were prepared in dichloroethane (DCE) at concentrations of 1×10^{-3} M.

Synthesis of Porphyrins. Control porphyrin **2a** was synthesized via a "3 + 1" condensation procedure[22] (cf. Scheme 1 and discussion below) as follows. First, tripyrrane **3** (231 mg, 492.5 mmol) was stirred in neat trifluoroacetic acid (2 mL) at room temperature (r.t.) under a nitrogen atmosphere for 10 min. The reaction was then diluted with 150 mL of dried, deaerated dichloromethane (DCM) and then treated with 2,5-diformylpyrrole **4a** (55 mg, 447.2 mmol). After stirring for 2 h at r.t., dichlorodicyanoquinone (DDQ) (152 mg, 669.6 mmol) was added. The reaction was stirred for an additional 30 min before 3.7 mL of triethylamine was added. The volatiles were then removed using a rotary evaporator. The desired porphyrin was purified over silica gel using DCM as the eluent. After removal of the solvent, the first, major red fraction was obtained as a red solid. Recrystallization from a mixture of dichloromethane/methanol (DCM/MeOH) then yielded porphyrin **2a** (36.5 mg, 14%) as a crystalline product. ^{1}H NMR (400 MHz, $CDCl_3$) δ 10.18 (s, 2H), 10.12 (s, 2H), 9.41 (s, 2H), 4.45 (t, J = 7.8, 4H), 4.12 (q, J = 7.6, 4H), 3.67 (s, 6H), 3.66 (s, 6H), 3.29 (t, J = 7.8, 4H), 1.93 (t, J = 7.6, 6H), −3.77 (s, 2H). ^{13}C NMR (101 MHz, $CDCl_3$) δ 174.2, 119.8, 101.4, 96.6, 52.4, 37.6, 22.5, 20.4, 19.2, 12.2. ESI MS (+): 567 $[M + H]^+$. HiRes MS ESI(+): found 567.2965, calc., for $C_{34}H_{39}N_4O_4^+$ 567.2971. High-performance liquid chromatography (HPLC) analysis confirmed the bulk purity of the product (99%) (see further descriptions in the Supporting Information).

Diiodoporphyrin ***2b***. In a vessel protected from ambient light, tripyrrane **3** (44 mg, 77.2 mmol) was stirred in neat trifluoroacetic acid (1 mL) at r.t. under a nitrogen atmosphere for 10 min. The reaction was then diluted with 8 mL of dry, deaerated DCM followed by treatment with 3,4-diiodo-2,5-diformylpyrrole **4b** (29 mg, 77.2 mmol). After stirring for 2 h at r.t., DDQ (18 mg, 79.3 mmol) was added. Then the reaction was stirred for an additional 30 min before 1.8 mL of triethylamine was added. The volatiles were removed using a rotary evaporator. The desired porphyrin was purified over silica gel using DCM as the eluent. After evaporative removal of the solvent, the first, major red fraction was obtained as a red solid, which was recrystallized from a mixture of DCM and MeOH; this yielded **2b** (34.2 mg, 54%) in the form of a red crystalline product. ^{1}H NMR (400 MHz, $CDCl_3$) δ 10.02 (s, 2H), 9.88 (s, 2H), 4.40 (t, J = 7.7, 4H), 3.98 (q, J = 7.6, 4H), 3.64 (s, 6H), 3.61 (s, 6H), 3.21 (t, J = 7.8, 4H), 1.87 (t, J = 7.6, 6H), −4.41 (s, 2H). ^{13}C NMR (101 MHz, $CDCl^3$) δ 173.9, 154.9, 151.6, 145.6, 137.1, 136.2, 136.1, 135.9, 108.3, 102.1, 97.1, 37.4, 30.39, 22.3, 20.5, 19.2, 12.2. MS ESI (+) 819 $[M + H]^+$. HiRes MS ESI(+): found 819.0894, calc. for $C_{34}H_{37}N_4O_4I_2^+$ 819.0899 (see more detailed descriptions in the Supporting Information).

Porphyrin ***1***. Deaerated toluene (10 mL), deaerated methanol (3 mL), and deaerated water (1 mL) were added to a mixture of diiodoporphyrin **2b** (28.5 mg, 34.8 mmol), 2-bithiophene boronic acid (29.3 mg, 139.5 mmol), $Pd(PPh_3)_4$ (4.0 mg, 3.5 mmol), and Na_2CO_3 (29.3 mg, 273 mmol) under a nitrogen atmosphere. The resulting reaction mixture was stirred at 80 °C for 10 h. The reaction mixture was then cooled to r.t. The aqueous layer was separated off and extracted with DCM (2 × 50 mL). The combined organic phases were dried over Na_2SO_4 and then filtered. The

dx.doi.org/10.1021/jp110482v |*J. Phys. Chem. C* 2011, 115, 2592–2599

volatiles were removed using a rotary evaporator. The desired porphyrin was purified over silica gel using DCM as the eluent. The first, major red fraction was obtained in the form of a red solid product after evaporative removal of the solvent. After recrystallization from a mixture of DCM/MeOH, product **1** was obtained as crystalline product (23.2 mg, 74%). ^{1}H NMR (400 MHz, $CDCl_3$) δ 10.31 (s, 2H), 10.01 (s, 2H), 7.62 (dd, J = 32.8, 3.2, 4H), 7.37 (dd, J = 31.4, 4.0, 4H), 7.14 (d, J=3.9, 2H), 4.41 (t, J = 7.5, 4H), 4.04 (q, J = 7.6, 4H), 3.68 (s, 6H), 3.59 (s, 6H), 3.27 (t, J = 7.6, 4H), 1.93 (t, J = 7.5, 6H), −3.71 (s, 2H). ^{13}C NMR (101 MHz, $CDCl_3$) δ 174.0, 145.3, 140.5, 138.4, 137.0, 136.6, 136.6, 136.5, 136.1, 131.7, 128.7, 125.3, 125.2, 125.1, 124.6, 100.7, 96.9, 52.5, 37.4, 22.4, 20.5, 19.2, 12.3. ESI MS (+): 896 $[M + H]^+$. HiRes MS ESI(+): found 895.2477, calc. for $C_{50}H_{47}N_4O_4S_4^+$ 895.2475. Elemental analysis calculated for $C_{50}H_{48}N_4O_4S_4$: C 67.09, H 5.18, N 6.26; found: C 67.12, H 5.47, N 5.97. This compound was further characterized via a single crystal X-ray diffraction analysis.

Characterization Methods. NMR spectra were recorded on a Varian Mercury 400 spectrometer. Low-resolution electrospray ionization (ESI) mass spectra were measured on an Agilent 6130 Quadrupole LC/MS spectrometer. High-resolution mass spectra were measured on a Varian 9.4T HiResESI-QFT ion cyclotron resonance mass spectrometer. Elemental analysis was performed at the Atlantic Microlab, Inc. Crystallographic data were collected on a Riau SCX-Mini diffractometer equipped with a Mercury CCD and a graphite monochromator using Mo Kα radiation (λ = 0.71073 Å). HPLC analysis was conducted on a Shimadzu HPLC system (LC-6AD liquid chromatograph, SIL-20AC auto sampler, DGU-20A5 degasser, SPD-M20A diode array detector) with a C18 reverse phase column and acetonitrile−water mixture as a mobile phase.

Preparation of TiO_2 Nanotubes/Ti Foil Substrate. The TiO_2 nanotubes were prepared using a previously reported procedure.[17] Briefly, anodic titania templates with a pore size of about 80−100 nm were grown on high purity titanium plates (0.25 mm thick, 99.5% purity) by constant voltage anodization at 20 V in ethylene glycol−water (99:1, volume ratio) with the addition of 0.5 wt % NH_4F at 20 °C for about 20 h. The resulting samples were then annealed at 450 °C in air for 3 h.

Preparation of Photosensitizer Arrays. A CH Instruments dispenser (model 1550, Austin, TX) was used to fabricate the photosensitizer arrays. It consists of a computer-controlled stepper-motor-operated XYZ stage with a piezoelectric dispensing tip (MicroJet AB-01-60, MicroFab, Plano, TX) attached to the head and a sample platform. The arrays were prepared by a procedure previously reported by our group.[7] Briefly, the TiO_2 nanotubes/Ti foil substrate was placed on the sample platform of the dispenser, and the XYZ stage moved the tip in a preprogrammed pattern, while programmed voltage pulses were applied to the dispenser to eject the requested number of drops (~100 pL each) of the precursor solution (dye solution) onto the TiO_2 nanotubes/Ti foil. The first dye (dye solution) was loaded and dispensed in a preprogrammed pattern onto the TiO_2 nanotubes/Ti foil substrate. After flushing and washing the piezodispenser several times, a second dye was loaded at the dispenser and dispensed into different positions than the first dye spots. The dye arrays were kept in air under ambient conditions to allow the solvent to evaporate.

Screening of the Array. The screening of the sensitizer arrays was performed by an optical fiber-modified SECM setup described in a previous publication.[13] Briefly, a 400 μm optical fiber (FT-400-URT, 3M, St. Paul, MN) coupled to a 150 W Xe lamp (Oriel) was fixed in the tip holder of a CHI model 900B SECM instrument. The prepared sensitizer arrays were placed in a Teflon cell with the sensitizer/TiO_2 nanotubes/Ti foil working electrode exposed at the bottom through a hole sealed with an O-ring (exposed area 1.0 cm^2). To test the effect of the dye sensitizer, a Pt wire counter electrode and an Ag wire quasi-reference electrode (AgQRE) were used to complete the three-electrode configuration. A 0.1 M tetrabutyl ammonium iodide (TBAI) in acetonitrile (MeCN) was used as the electrolyte and as an electron donor. The optical fiber was positioned perpendicular to the array at a distance of about 100 μm and scanned across the surface at a speed of 500 μm/s (SECM setting 50 μm/0.1 s). A 420 nm long-pass wavelength filter was used to block the UV light in visible light illumination experiments. During the scan, a given potential was applied to the working electrode array using the SECM. The measured photocurrent during the scan produced a color-coded, two-dimensional image.

Preparation and PEC Measurements of Bulk Samples. The annealed TiO_2 nanotubes/Ti foil electrodes were immersed in an ethanol solution containing 2×10^{-4} M N719, DCE solution containing 2×10^{-4} M porphyrin **1**, and control porphyrin **2a** for at least 24 h, respectively. The resulting thin film was used as a photoworking electrode with 0.2 cm^2 geometrical area exposure to electrolyte solution and light irradiation. Light irradiation was performed through the electrolyte solution using a 150 W Xe lamp with an incident light intensity of about 100 mW/cm^2. A UV cutoff filter (>420 nm) was used for visible light irradiation. The PEC measurements were carried out in a 0.1 M TBAI in MeCN.

RESULTS AND DISCUSSION

Sensitizer Design Considerations. Although porphyrins have not shown the desired efficiency for use in practical devices, the large number of previous studies of porphyrins led us to consider how elaboration of a porphyrin with electron-rich substituents, in particular bithiophenes, might affect its behavior as a sensitizer. To test this hypothesis, we set out to create porphyrins bearing this functionality. However, in considering the placement of these electron-rich groups, we wanted to avoid substitution at the *meso* or bridging carbon, positions. In porphyrins, the electron density in the highest occupied molecular orbitals (HOMOs) is generally higher on the meso positions compared to the rest of the macrocycle. This makes these sites the more reactive ones in electrophilic substitution reactions (halogenation, nitration, etc.).[18] However, substitution at the *meso* substituents, for example, with phenyl groups, generally places the substituents in a geometry that is orthogonal or at least tilted away from the plane of the porphyrin (i.e., a high dihedral angle). This tends to reduce the extent of coupling with the porphyrin conjugation pathway.[19] Therefore, we sought a general and easy way to functionalize porphyrins at the so-called β-pyrrolic positions. Dihalogenated meso-free porphyrins seem especially appealing precursors for accomplishing this goal. Halogen atoms in the porphyrin periphery have been shown to act as effective coupling partners in Suzuki−Miyaura reactions,[20] making β-dihalogenated porphyrins attractive intermediates for the preparation of the targeted bis-bithiophene functionalized porphyrins sought in the context of this study.

Although halogenated *meso*-free porphyrins have been reported, their synthesis is tedious and utilizes sensitive material (dibromopyrroles or dibromotripyrranes).[21] Therefore, we developed an alternative approach based on a so-called "3 + 1" condensation; this chemistry is discussed further below.

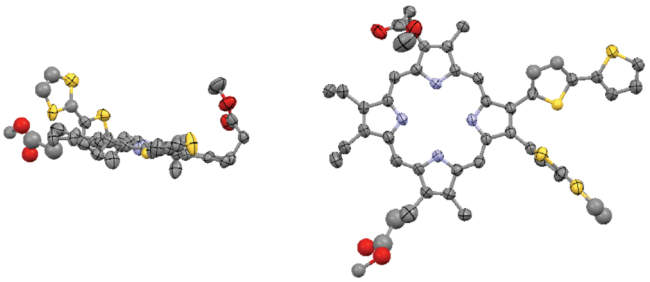

Figure 1. Top and side views of a single crystal X-ray diffraction structure of porphyrin **1** showing two orientations of the bithiophene substituents. All hydrogen atoms are omitted for clarity. Thermal ellipsoids are scaled to the 50% probability level.

Synthesis. Porphyrin **1** was synthesized from porphyrin **2b** as shown in Scheme 1. Porphyrin **2b**, in turn, was prepared from the known diiodopyrrole **4b** and diacid **3** via a "3 + 1" procedure analogous to that described in the literature.[22,23] Specifically, condensation of **3** and **4b** in neat trifluoroacetic acid (TFA) produced the reduced, porphyrinogen form of **2b**. Treatment with DDQ then gave diiodoporphyrin **2b**. Suzuki coupling between **2b** and bithiophene boronic acid then produced porphyrin **1** in 74% yield.

We also prepared the unsubstituted porphyrin **2a** as a control compound. While similar porphyrins are known,[22] this specific compound does not appear to have been reported previously.

A single crystal of **1** suitable for X-ray diffraction analysis was obtained by recrystallizing from a DCM/MeOH mixture. Although disorder in the crystal packing was observed in the resulting structure, it was found that, at least in the solid state, one bithiophene moiety is orthogonal to the porphyrin, whereas the other is fairly coplanar with this latter macrocyclic ring (Figure 1). Additional crystallographic data of **1** are also summarized in the Supporting Information.

Photoelectrochemistry. To show that the SECM technique can be used to test the photoeffects of the dyes, we chose a commercially available ruthenium dye N719 to prepare the arrays on the TiO_2 nanotube substrate. Ruthenuim complexes, such as the N3, N719, and C101 dyes, are among the most efficient photosensitizers to date.[24−27] We chose TiO_2 as the target material because it is used in nanoparticle (NP) form in most DSSCs and has a large band gap that gives rise to little visible response. We thus considered it likely that vertically oriented anodic TiO_2 films might be appropriate for enhancing electron transport in TiO_2 films.[28] TiO_2 nanotube electrodes possess a relatively large surface area and the quantity of dye molecules absorbed onto the nanostructures is considerably increased relative to what is true for NP TiO_2 films. As a result, the efficiency of charge collection is generally much better than that of NP films. There are several studies using TiO_2 nanotubes as the electrode in DSSCs.[29,30] The hollow nature of these tubes makes both inner and outer surface areas accessible for modification with sensitizing dyes. The un-oxidized titanium base that supports the nanotube arrays facilitates electrical contact to collect the photogenerated charge carriers. The 10 μm thick nanostructured TiO_2 film is now being used as an electron transporting layer which consists typically of interconnected nanometer-sized TiO_2 particles.[28] Figure 2 shows a scanning electron microscopy (SEM) image of a typical substrate of TiO_2 nanotubes (thickness ~5 μm) with a ~60 nm inner diameter and a ~80 nm outer diameter. It would probably also be possible to use nanoporous TiO_2 or ZnO as conventionally used in DSSCs as a substrate for these arrays.

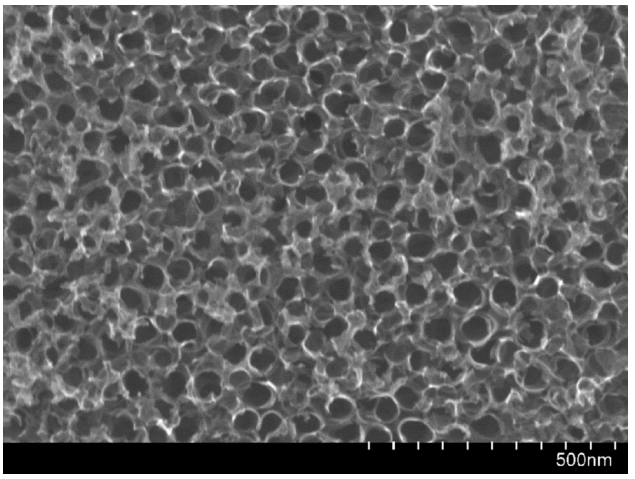

Figure 2. SEM image of TiO_2 nanotubes anodized at 20 V in ethylene glycol/water (99:1, volume ratio) with the addition of 0.5 wt % NH_4F.

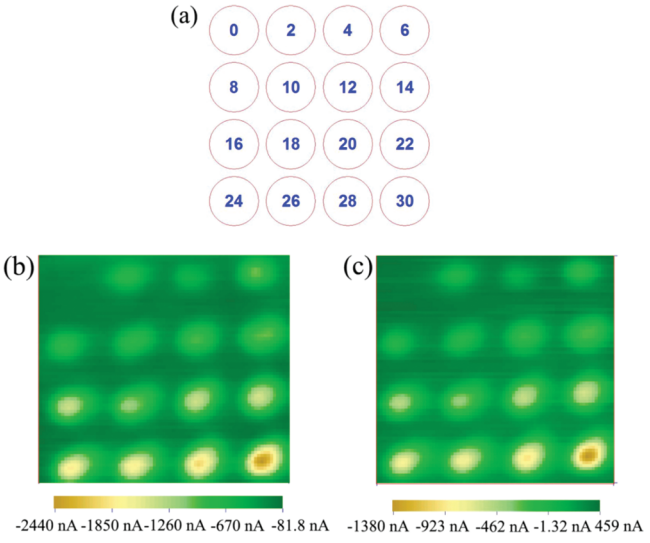

Figure 3. (a) Dispensed pattern of a N719 sensitizer array. Shown are number of drops dispensed at a given location. SECM images of N719 sensitizer on TiO_2 nanotubes/Ti foil at an applied potential of 0.2 V vs AgQRE under (b) UV−visible and (c) visible light (λ > 420 nm). Scan rate: 500 μm/s (SECM setting 50 μm/0.1 s); solution, 0.1 M TBAI in MeCN.

Screening of Dye Photosensitizer Array. Figure 3a shows the array pattern created by a different number of drops of dispensed solution. The numbers inside the circles represent the number of drops dispensed for that spot. For example, the spot at the upper left corner has no dye, while the spot at the bottom right corner contains 30 drops of the same dye. Figure 3b,c show the SECM images obtained for a sensitizer array consisting of dye N719. The applied potential was 0.2 V versus AgQRE, when the solution contained 0.1 M TBAI in MeCN. As shown in this figure, the anodic photocurrent increased with the number of N719 dye drops. The same trend was seen at higher bias potentials (not shown). The maximum photocurrent of the spot showed a 30 times larger current compared to the pure TiO_2 nanotubes (substrate), 2240 nA versus 81.8 nA, under UV−visible irradiation. Note that, under visible light irradiation (λ > 420 nm), the background current changed to a positive (reduction) current,

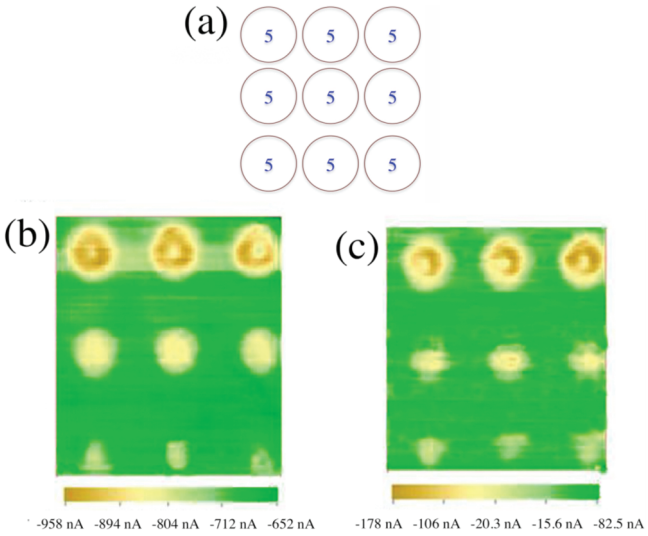

Figure 4. (a) Dispensed pattern of three different kinds of dye arrays. SECM images of three different kinds of dyes on TiO_2 nanotubes/Ti foil at an applied potential of 0.5 V vs an AgQRE under (b) UV−visible and (c) visible light. Scan rate: 500 μm/s (SECM setting 50 μm/0.1 s); solution, 0.1 M TBAI in MeCN.

due to the reduction of photogenerated iodine on the TiO_2 substrate. Another contribution to this change in background current is the reduction of O_2 dissolved in the electrolytes under the conditions used to screen the arrays. Under both UV−visible light and visible light irradiation, the spots with larger amounts of dye displayed larger photocurrents in the range of dye deposited. Note that there is an adsorption limit for the TiO_2 nanotube substrate. When the amount of dye reached the limit or exceeded the limit, the dye tended to desorb from the TiO_2 surface. Such tendencies were noted in our experiments.

Numerous papers have discussed the N719 dye used in the DSSC field, with a number of substrate materials having been sensitized by this ruthenium complex, including TiO_2 nanotubes,[30] as well as $SrTiO_3$[31] and Zn_2SnO_4[32] substrates. The purpose of our experiments using TiO_2 nanotubes and N719 was to test whether a modified SECM technique could be used to effect the rapid screening of sensitizers; N719 was thus chosen as a positive control in these studies because it is a widely known, efficient sensitizer.

After proving that the SECM technique can be used to monitor this particular photosensitizer, we sought to test the new porphyrin dyes. Toward this end, the bisthiophene-substituted porphyrin **1** was prepared, as noted above. SECM was then used to compare its efficiency and that of a porphyrin-based, negative control system, **2a**, with that of N719. Figure 4a shows three different kinds of dye array patterns. The numbers inside the circles represent the number of drops dispensed for that spot. The first row is pure N719, the second row is pure porphyrin **1**, and the last row is pure control porphyrin **2a**. Figure 4b,c show the images obtained for the sensitizer arrays consisting of N719, porphyrin **1**, and control porphyrin **2a**. The applied potential was 0.5 V versus AgQRE, and the solution was 0.1 M TBAI in MeCN.

As seen in Figure 4b,c, the modified SECM method makes it easy to compare the relative photocurrents of the dyes. As noted above, the iodine photogenerated by irradiation of dyes is reduced on TiO_2 at a sufficiently small bias so that only a low background reduction current is obtained. To avoid or decrease this small reduction current further, we applied a more positive potential

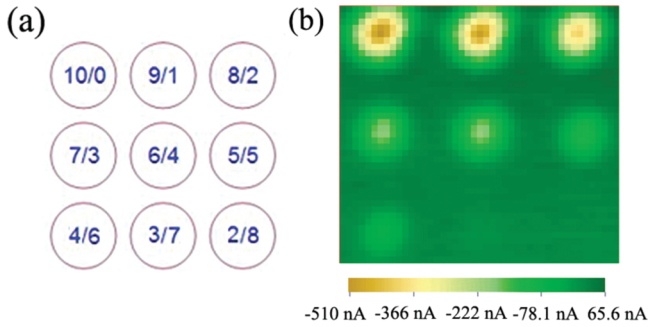

Figure 5. (a) Dispensed pattern of dye arrays. The first spot in the first row is 100% N719. The first and second numbers inside each circle represent the number of drops of N719 and porphyrin **1**, respectively. (b) SECM image of dyes on TiO_2 nanotubes/Ti foil at an applied potential of 0.2 V vs an AgQRE under visible light. Scan rate: 500 μm/s (SECM setting 50 μm/0.1 s); solution, 0.1 M TBAI in MeCN.

(0.5 V vs AgQRE) when screening the arrays. At this potential bias, the ruthenium-based sensitizer N719 displayed average anodic photocurrents of 945 and 170 nA under UV−visible and visible illumination, respectively, compared to porphyrin **1**, with average photocurrents of 850 and 74 nA and the control porphyrin **2a** with average photocurrents of 791 nA and 13 nA, respectively, upon irradiation with UV−visible and visible light. The TiO_2 nanotubes have a high response in the UV region (λ < 420 nm), so the response indicated that under UV−visible light illumination is high because of the direct TiO_2 response.[17] Thus the sensitized photooxidation current under visible light illumination is more diagnostic of the relative efficiency. By comparing the photocurrent values of the three different dyes under visible light irradiation, it becomes possible to rank in order the relative efficiencies of the three photosensitizers studied here (N719, porphyrin **1**, and porphyrin **2a**). Clearly N719 was the most effective sensitizer, but the ruthenium-free porphyrin **1** produced a reasonable response, while the negative control, **2a**, produced a photocurrent only 25−35% of that of porphyrin **1**. Note that, for these studies, the concentrations of porphyrin **1** and control porphyrin **2a** were 5 times larger than that of N719 and the results have been normalized to take this into account. On the basis of the above analysis, we thus conclude that the SECM technique is a fast and convenient way to compare the relative sensitization efficiencies of different dyes.

Previously, we used the SECM technique to investigate the effect of metal or nonmetal element dopants on known photocatalysts[13,17] as well as for binary metallic electrocatalysts.[7−10] The results obtained led us to consider that this method could be used to test whether there is a synergistic benefit when two kinds of dyes are used together. Both N719 and porphyrins represent established dyes for spectral sensitization, as noted in the introductory portions of this paper. Therefore, we chose N719 and porphyrin **1** as test systems with which to probe whether the SECM technique could be used to observe an improved effect with mixtures of the dyes. Figure 5a displays the dispensed pattern. The first spot in row 1 consists of 100% N719. The first number in the circles is the number of drops of an ethanol solution containing 0.2 mM N719 used to make the spot in question, whereas the second number is the number of drops of a 0.2 mM solution of porphyrin **1** in DCE used on the same spot. Figure 5b displays the photocurrent obtained at a 0.2 V applied potential in the presence of I^- as the electron donor. However, in this case the highest photocurrent was found with a molar ratio of N719:porphyrin **1** of 10:0, that is, spots containing pure (100%) N719 displayed the best

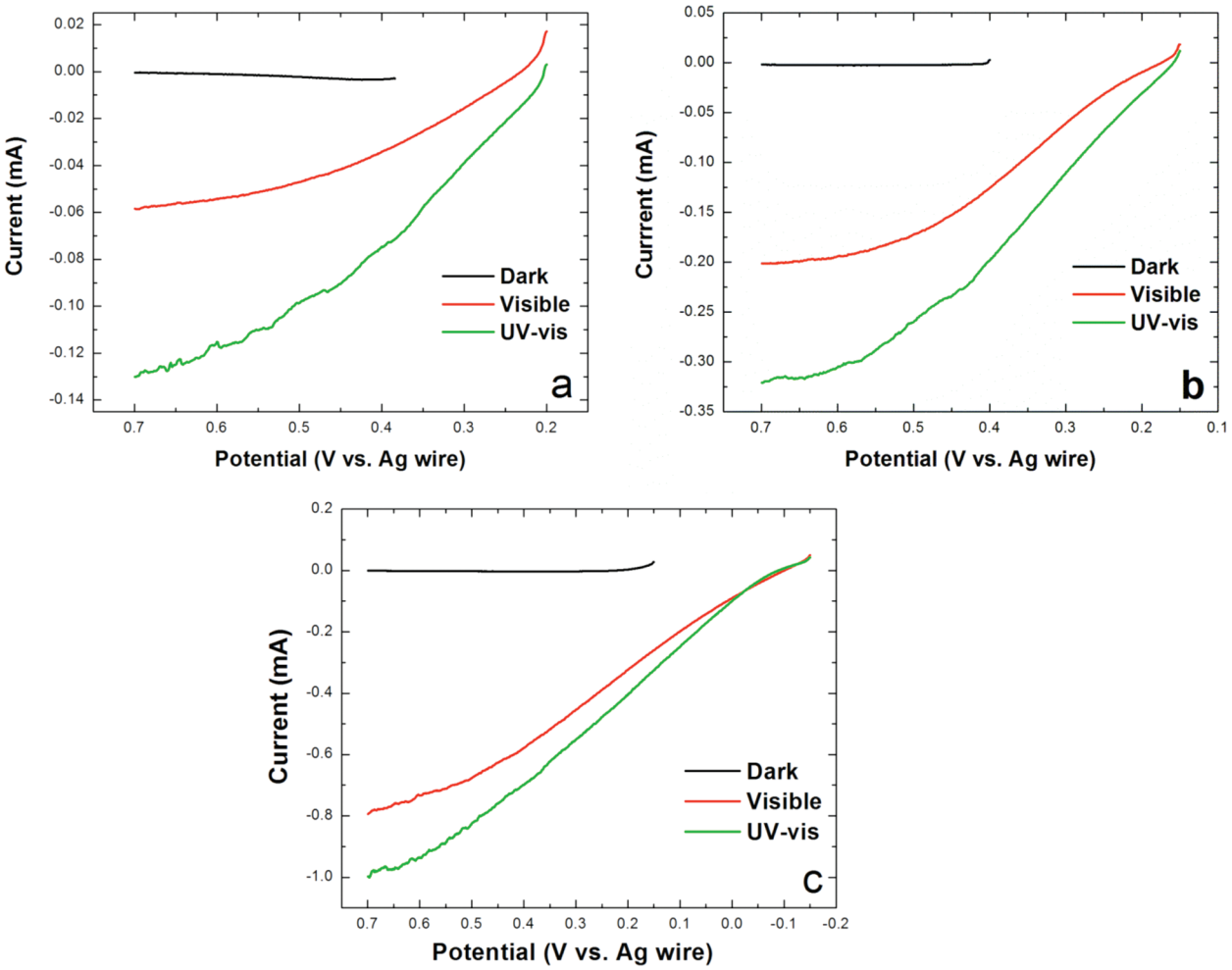

Figure 6. Linear sweep voltammograms (LSVs) of (a) control porphyrin and (b) porphyrin **1** and (c) N719 bulk films in MECN with 0.1 M TBAI as sacrificial reagent under dark, visible, and UV−visible light irradiation. Scan rate: 20 mV/s. Exposed electrode area, ~0.2 cm^2.

photocatalysis. As the amount of porphyrin **1** increased and the N719 decreased, the photocurrent of the spots decreased. This decrease is an accord with the relative photosensitization ability of these two dyes, as illustrated in Figure 4. While no particular synergy between the two dyes was found, SECM can be used to monitor mixtures of two or more dyes, particularly where one can absorb light over a larger portion of the spectrum.

Bulk Film Study. To confirm the utility of the SECM technique for preliminary screens of dye efficacy, PEC measurements were carried out with bulk films. We prepared dye bulk films using the immersion method as described in the Experimental Section. PEC measurements were then carried out with these films in a three-electrode cell containing 0.1 M TBAI in MeCN under UV−visible and visible light illumination. Figure 6 shows the linear sweep voltammograms (LSVs) of control porphyrin **2a**, porphyrin **1**, and N719 bulk films in 0.1 M TBAI in MeCN under conditions of UV−visible and visible light irradiation and in the dark, with the potential being swept from 0.15 to 0.7 V vs an AgQRE for both the control porphyrin and porphyrin **1** bulk films. For the bulk film produced from dye N719, the potential was swept from −0.15 to 0.7 V versus the AgQRE.

As shown in Figure 6, the onset photocurrent potential was about 0.20, 0.15, and −0.10 V for control porphyrin **2a**, porphyrin **1**, and dye N719, respectively. The open circuit photopotential under visible light irradiation was about 0.25, 0.20, and −0.10 V versus an AgQRE for control porphyrin **2a**, porphyrin **1**, and dye N719, respectively, indicating that, among those three dyes tested, dye N719 had the highest open circuit photovoltage with respect to I^-/I_3^- redox potential on a Pt counter electrode for a two-terminal PEC device. Notice that the first and second peak potentials for the oxidation of I^- on Pt in MeCN occur at 0.047 and 0.363 V versus Ag/Ag^+(0.01 M).[33] The bulk film produced from dye N719 showed the highest photocurrents under both UV−visible and visible irradiation. The bulk film prepared from porphyrin **1** displayed a higher photocurrent than that of the control porphyrin bulk film made from **2a**. The enhancements in the sensitized photocurrent seen for films made with the N719 dye or porphyrin **1** relative to this latter control system (i.e., **2a**) were comparable to what was seen in the case of the SECM measurements.

The UV−visible absorption spectra of porphyrin **1**, control porphyrin **2a**, and N719 were measured in DCE (Figure 7). The peak positions and molar absorption coefficients (ε) of the Soret and Q bands are listed in Table 1. As shown in Figure 7, the UV−visible absorption spectra of porphyrin **1** and control porphyrin **2a** exhibit typical strong Soret bands near 400 nm and weaker Q bands in the region of 500−650 nm. The Soret band of porphyrin **1** is red-shifted and broadened relative to that of control porphyrin **2a**, a finding that is likely due to the presence of the

dx.doi.org/10.1021/jp110482v |*J. Phys. Chem. C* 2011, 115, 2592–2599

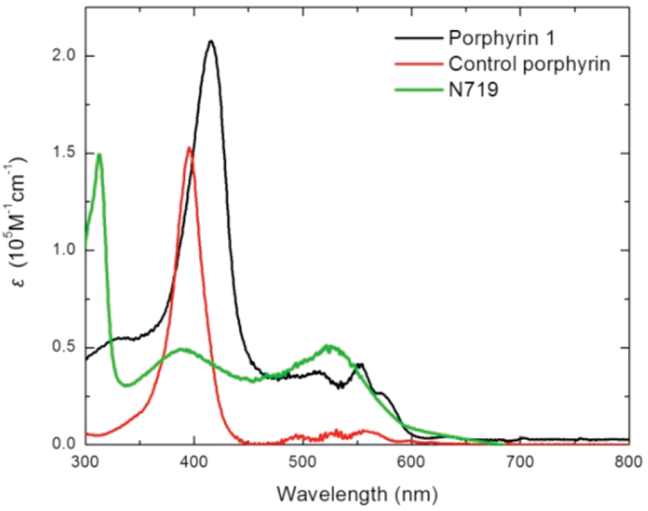

Figure 7. UV−visible absorption spectra of porphyrin **1**, control porphyrin **2a**, and dye N719 measured in dichloroethane.

Table 1. Spectroscopic Data for Porphyrin 1, Control Porphyrin 2a, and N719 Recorded in DCE

species	λ_{abs}/nm (ε/10^3 M^{-1}cm^{-1})
porphyrin **1**	416 (207.7)
	494 (35.8)
	510 (38.2)
	553 (41.6)
control porphyrin **2a**	396 (152.8)
	493 (5.3)
	535 (6.7)
	555 (7.4)
N719	313 (149.3)
	387 (49.2)
	529 (50.2)

bithiophene substituents. Although the Q-band of the control porphyrin is red-shifted in comparison with that of porphyrin **1**, the molar absorption coefficient (ε) of the Q-band of control porphyrin **2a** is much lower. The molar absorption coefficients at the Soret bands of the control porphyrin are ∼70% of that for porphyrin **1**. More importantly, the integrated values of the molar absorption coefficients for the Q bands (500−700 nm) of porphyrin **1** are nearly seven times larger than those for the control porphyrin **2a**. This means that, compared to **2a**, porphyrin **1** is more attractive for the purpose of harvesting solar energy. Specifically, porphyrin **1** can absorb much more incident light in the visible region than can control porphyrin **2a**. However, porphyrin **1** is still not as effective as dye N719; this latter system is characterized by three typical absorption peaks, as shown in Figure 7. The maxima of these peaks appear at ca. 313, 387, and 529 nm, respectively. The integrated value of their molar absorption coefficients over the 500−700 nm spectral regions is 1.3 times larger than what is found in the case of porphyrin **1**.

CONCLUSIONS

Reported here is a new synthetic route to *meso*-unsubstituted porphyrins bearing β-substituents. This method, which relies on the construction of a bis-iodo β-functionalized porphyrin precursor and its subsequent elaboration, was used to prepare the bis-bithiophene substituted porphyrin **1**. This new porphyrin was shown to act as an efficient sensitizer for use in DSSCs. The present study also serves to highlight the utility of a modified SECM-based technique, which permits a rapid, initial evaluation of photosensitizers for use in DSSC applications. This SECM technique is attractive in that it should not only permit the facile identification of individual new dyes but also permit the potential synergetic effects of multiple dyes to be easily tested. In addition to the latter benefits, the present study serves to underscore the combination of a piezodispenser and SECM as a means of fabricating quickly, easily, and in a reproducible fashion ca. 400 μm spot-size sensitizer arrays and evaluating their sensitization effects.

ASSOCIATED CONTENT

Supporting Information. HPLC and NMR data, elemental analysis, crystallographic analysis of **1**, and its raw crystallographic data (11p82.cif). This material is available free of charge via the Internet at http://pubs.acs.org.

AUTHOR INFORMATION

Corresponding Author

*E-mail: sessler@mail.utexas.edu, ajbard@mail.utexas.edu.

ACKNOWLEDGMENT

This work was supported by the National Science Foundation (Grant CHE 0730053 to J.L.S. and CHE 0934450 to A.J.B.) and the Robert A. Welch Foundation (Grants H-F-0037, F-0021, and F-1018 to the Center for Electrochemistry, A.J.B., and J.L.S., respectively). F.Z. thanks the National Scholarship Fund of the China Scholarship Council for support and her advisor in China Prof. Yansheng Yin from Shanghai Maritime University.

REFERENCES

(1) Nazeeruddin, M. K.; Angelis, F. D.; Fantacci, S.; Selloni, A.; Viscardi, G.; Liska, P.; Ito, S.; Takeru, B.; Grätzel, M. *J. Am. Chem. Soc.* **2005**, *127*, 16835.

(2) Gao, F.; Wang, Y.; Shi, D.; Zhang, J.; Wang, M.; Jing, X.; Humphry-Baker, R.; Wang, P.; Zakeeruddin, S. M.; Grätzel, M. *J. Am. Chem. Soc.* **2008**, *130*, 10720.

(3) Chen, C. Y.; Wang, M. K.; Li, J. Y.; Pootrakulchote, N.; Alibabaei, L.; Ngoc-le, C.; Decoppet, J. D.; Tsai, J. H.; Grätzel, C.; Wu, C. G.; Zakeeruddin, S. M.; Grätzel, M. *ACS Nano* **2009**, *3*, 3103–3109.

(4) Mozer, A. J.; Griffith, M. J.; Tsekouras, G.; Wagner, P.; Wallace, G. G.; Mori, S.; Sunahara, K.; Miyashita, M.; Earles, J. C.; Gordon, K. C.; Du, L.; Katoh, R.; Furube, A.; Officer, D. L. *J. Am. Chem. Soc.* **2009**, *131*, 15621.

(5) Jasieniak, J.; Johnston, M.; Waclawik, E. R. *J. Phys. Chem. B* **2004**, *108*, 12962.

(6) See, for example, *Scanning Electrochemical Microscopy*, 1st ed.; Bard, A. J., Mirkin, M. V., Eds.; Marcel Dekker: New York, 2001.

(7) Fernández, J. L.; Walsh, D. A.; Bard, A. J. *J. Am. Chem. Soc.* **2005**, *127*, 357–365.

(8) Walsh, D. A.; Fernández, J. L.; Bard, A. J. *J. Electrochem. Soc.* **2006**, *153*, E99.

(9) Fernández, J. L.; White, J. M.; Sun, Y. M.; Tang, W. J.; Henkelman, G.; Bard, A. J. *Langmuir* **2006**, *22*, 10426–10431.

(10) Fernández, J. L.; Raghuveer, V.; Manthiram, A.; Bard, A. J. *J. Am. Chem. Soc.* **2005**, *127*, 13100–13101.

(11) Minguzzi, A.; Alpuche-Aviles, M.; Rodríguez López, J.; Rondinini, S.; Bard, A. J. *Anal. Chem.* **2008**, *80*, 4055–4064.

(12) Liu, W.; Ye, H.; Bard, A. J. *J. Phys. Chem. C* **2010**, *114*, 1201–1207.
(13) Lee, J.; Ye, H.; Pan, S.; Bard, A. J. *Anal. Chem.* **2008**, *80*, 7445–7450.
(14) Knizhnikov, V. A.; Borisova, N. E.; Yurashevich, N. Ya.; Popova, L. A.; Chernyadèv, A. Yu.; Zubreichuk, Z. P.; Reshetova, M. D. *Russ. J. Org. Chem.* **2007**, *43*, 855–860.
(15) Voloshchuk, R.; Gałęzowski, M.; Gryko, D. T. *Synthesis* **2009**, 1147.
(16) Kim, D.-S.; Ahn, K. H. *J. Org. Chem.* **2008**, *73*, 6831–6834.
(17) Zhang, F.; Chen, S. G.; Yin, Y. S.; Lin, C.; Xue, C. R. *J. Alloys Compd.* **2010**, *490*, 247–252.
(18) Ghosh, A. *The Porphyrin Handbook*; Kadish, K. S., Smith, K. M., Guilard, R., Eds.; Academic Press: New York, 2000; Vol. 7, pp 1−38.
(19) Medforth, C. J.; Berber, D.; Smith, K. M.; Shelnutt, J. A. *Tetrahedron Lett.* **1990**, *31*, 3719–3722.
(20) Zhou, X.; Tse, M. K.; Wan, T. S. M.; Chan, K. S. *J. Org. Chem.* **1996**, *61*, 3590–3593.
(21) Siri, O.; Smith, K. M. *Tetrahedron Lett.* **2003**, *44*, 6103–6105.
(22) Sessler, J. L.; Genge, J. W.; Urbach, A. *Syn. Lett.* **1996**, 187–188.
(23) Lin, V.; Lash, L. D. *Tetrahedron Lett.* **1995**, *36*, 9441–9444.
(24) Wang, Q.; Ito, S.; Grätzel, M.; Fabregat-Santiago, F.; Mora-Seró, I.; Bisquert, J.; Bessho, T.; Imai, H. *J. Phys. Chem. B* **2006**, *110*, 25210–25221.
(25) Grätzel, M. *Nature* **2001**, *414*, 338–344.
(26) Campbell, W. M.; Burrell, A. K.; Officer, D. L.; Jolley, K. W. *Coord. Chem. Rev.* **2004**, *248*, 1363–1379.
(27) Nazeeruddin, M. K.; De Angelis, F.; Fantacci, S.; Selloni, A.; Viscardi, G.; Liska, P.; Ito, S.; Takeru, B.; Grätzel, M. *J. Am. Chem. Soc.* **2005**, *127*, 16835–16847.
(28) Adachi, M.; Murata, Y.; Okada, I.; Yoshikawa, S. *J. Electrochem. Soc.* **2004**, *150*, G488.
(29) Kang, S. H.; Kim, J. Y.; Kim, Y.; Kim, H. S.; Sung, Y. E. *J. Phys. Chem. C* **2007**, *111*, 9614–9623.
(30) Chen, C. C.; Chung, H. W.; Chen, C. H.; Lu, H. P.; Lan, C. M.; Chen, S. F.; Luo, L. Y.; Hung, C. S.; Diau, E. W. G. *J. Phys. Chem. C* **2008**, *112*, 19151–19157.
(31) Yang, S. M.; Kou, H. Z.; Wang, J. C.; Xue, H. B.; Han, H. L. *J. Phys. Chem. C* **2010**, *114*, 4245–4249.
(32) Tan, B.; Toman, E.; Li, Y. G.; Wu, Y. Y. *J. Am. Chem. Soc.* **2007**, *129*, 4162–4163.
(33) Kadar, M.; Takats, Z.; Karancsi, T.; Farsang, G. *Electroanalysis* **1999**, *11*, 809–813. We have not determined the potential difference between the AgQRE we used and an Ag/Ag^{+}(0.01 M) reference electrode. In the presence of 0.1 M I^{-}, the AgQRE is perhaps acting as an Ag/AgI (0.1 M I^{-}) quasi reference electrode.